Available online at www.sciencedirect.com
ScienceDirect
Chemical Physics 330 (2006) 118–129
Chemical Physics
www.elsevier.com/locate/chemphys

Absorption and emission spectroscopic characterization of platinum-octaethyl-porphyrin (PtOEP)

A.K. Bansal [a], W. Holzer [a], A. Penzkofer [a,*], Taiju Tsuboi [b]

[a] *Institut II – Experimentelle und Angewandte Physik, Universität Regensburg, Universitätsstrasse 31, D-93053 Regensburg, Germany*
[b] *Faculty of Engineering, Kyoto Sangyo University, Kamigamo, Kita-ku, Kyoto 603-8555, Japan*

Received 15 March 2006; accepted 2 August 2006
Available online 4 August 2006

Abstract

The absorption and emission spectroscopic behaviour of the platinum complexed porphyrin PtOEP (platinum-octaethyl-porphyrin) is studied at room temperature. Liquid solutions, doped films, and a neat film are investigated. The absorption cross-section spectra including singlet–triplet absorption, the triplet–singlet stimulated emission cross-section spectra, the phosphorescence quantum distributions, the phosphorescence quantum yields, and the phosphorescence signal decays are determined. In the neat film a red-shifted phosphorescent excimer emission is observed. In diluted solid solution (polystyrene and dicarbazole-biphenyl films) as well as in de-aerated liquid solutions (tetrahydrofuran, toluene, chloroform) high phosphorescence quantum yields are obtained. In air-saturated liquid solutions, the phosphorescence efficiency is reduced by oxygen quenching. At intense short-pulse laser excitation the phosphorescence lifetime is shortened by triplet–triplet annihilation. No amplification of spontaneous emission was observed.

Keywords: Organometallic complex; PtOEP; Platinum-octaethyl-porphyrin; Doped film; Neat film; Liquid solutions; Phosphorescence quantum yield; Phosphorescence lifetime; Singlet–triplet absorption; Stimulated emission cross-section; Triplet–triplet annihilation; Amplified spontaneous emission

1. Introduction

Phosphorescent materials like lanthanide complexes [1], purely organic phosphors [2], and organometallic phosphors [3] gain importance in organic light emitting diodes (OLEDs) [4] because of higher potential efficiency than singlet emitters. In organic materials, one quarter of electrons is excited to the singlet system and three quarters are excited to the triplet system by electrical pumping. In phosphorescent materials, strong intersystem-crossing transfers the singlet excited molecules to the triplet system, resulting in an accumulation of all excited molecules in the triplet system. In the group of organometallic complexes, especially porphyrin platinum complexes such as platinum-octaethyl-porphyrin (PtOEP) [5–14] and phenylpyridine iridium complexes such as $Ir(ppy)_3$ [15–29] are the most widely used phosphorescent OLED materials. In an OLED containing 6 wt% PtOEP in CBP (4,4′-*N*,*N*′-dicarbazole-biphenyl) an external light emitting quantum efficiency of 5.6% (internal quantum efficiency 32%) at low brightness was achieved [9].

In PtOEP the fluorescence is strongly quenched by efficient S_1–T_1 singlet–triplet intersystem crossing due to enhancement of spin–orbit coupling by the heavy atom effect of Pt [30–34]. The singlet–triplet transition dipole moments are enhanced by the same effect (mixing of singlet and triplet states [35]). This strongly shortens the T_1 radiative lifetime, $\tau_{rad,P}$, of PtOEP to the 100–200 μs range [10,30,32,35]. The T_1–S_0 intersystem crossing (i.e. non-radiative relaxation from T_1 state to the ground state) is moderate leading to efficient phosphorescence quantum efficiency even at room temperature [10,30,32,35] in de-aerated liquid solutions [30] and in solid matrices [32,34,36–39]. The phosphorescence of PtOEP is effectively

* Corresponding author. Tel.: +49 941 943 2107; fax: +49 941 943 2754.
E-mail address: alfons.penzkofer@physik.uni-regensburg.de (A. Penzkofer).

0301-0104/$ - see front matter © 2006 Elsevier B.V. All rights reserved.
doi:10.1016/j.chemphys.2006.08.002

quenched by molecular oxygen [$T_1(PtOEP)+{}^3\Sigma_g^-(O_2) \rightarrow S_0(PtOEP)+{}^1\Delta_g(O_2)$] (for molecular oxygen quenching see [40]). PtOEP immobilized in oxygen permeable polymers is applied for oxygen sensing [32,36–39,41–44].

At high PtOEP concentration (>1.6 wt%) luminescence reduction was reported due to luminescence self-quenching [45]. In neat films of PtOEP the phosphorescence spectrum was found to be strongly red-shifted [33,46,47]. It is thought that aggregation occurs [46] leading to triplet dimeric excitons [33,47] (phosphorescent excimers [48–51]) which cause the solid-state neat film behaviour.

An optical characterization (absorption spectra and circular dichroism spectra) of PtOEP films over a wide temperature range was carried out [52], and the optical constants (refractive index and extinction coefficient) of PtOEP in single-layer light emitting diodes were determined [53]. The energy transfer dynamics from luminescent hosts to the phosphorescent PtOEP guest in thin films was studied for PtOEP emitter performance improvement [54–58].

In this paper, we study the absorption and emission behaviour of platinum(II)-2,3,7,8,12,13,17,18-octaethyl-21*H*,23*H*-porphyrin [Pt(II)octaethyl-porphyrin, PtOEP] at room temperature in neat film form, in liquid organic solution (solvents: tetrahydrofuran, toluene, and chloroform), in polystyrene films, and in a 4,4′-*N*,*N*′-dicarbazole-biphenyl (CBP) film. CBP is used in OLEDs as hole-transport material [4]. The fluorescence spectrum and phosphorescence spectrum of CBP is found in [59,54], respectively. Polystyrene is often used as host material for phosphorescent oxygen sensors [32,36–39,41–44]. The structural formulae of PtOEP, CBP, and polystyrene are shown in Fig. 1.

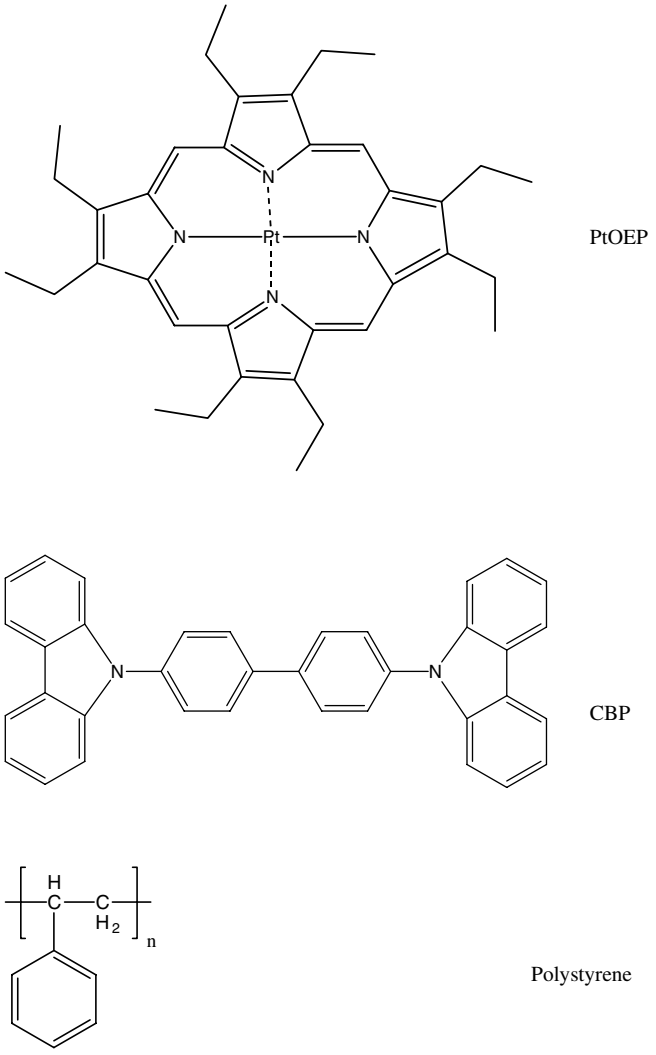

Fig. 1. Structural formulae of Pt-octaethyl-porphyrin (PtOEP, molar mass $M_m = 727.84\ g\ mol^{-1}$, sum formula $C_{36}H_{44}N_4Pt$), 4,4′-*N*,*N*′-dicarbazole-biphenyl (CBP, $M_m = 484.6\ g\ mol^{-1}$), and polystyrene (molar mass of repeat unit $M_{RU} = 104.15\ g\ mol^{-1}$).

2. Experimental

The metal complex PtOEP was purchased from Frontier Scientific, Logan, Utah, USA. CBP was delivered by Syn-Tec GmbH, Wolfen, Germany. Polystyrene (PS, molar mass 45,000 g mol^{-1}) and the solvents tetrahydrofuran (THF), toluene, and chloroform were purchased from Aldrich Co., Germany. All compounds were used as supplied without further purification. A 65 nm thick PtOEP neat film on a quartz glass substrate was prepared by vapour deposition.

The PtOEP/CBP and the PtOEP/PS films were prepared by spin-coating the appropriate solutions on optical glass substrates under ambient atmospheric conditions. Both the solutions and the substrates were heated up to 80 °C for the spin coating. The films containing 8.4 wt% PtOEP in CBP were prepared by dissolving 3.36 mg PtOEP and 36.64 mg CBP in 1 ml THF, and spin-coating the solution on the heated substrate at a speed of 1600 rpm. The PtOEP/PS films were made by spin coating the solutions on the heated substrate at a speed of 2000 rpm. For the films containing 1 wt% PtOEP 4 mg PtOEP and 396 mg PS were dissolved in 1 ml THF, for the films containing 4 wt% PtOEP 8.8 mg PtOEP and 211.2 mg PS were dissolved in 1 ml THF, while for the films containing 8 wt% PtOEP 6.4 mg PtOEP and 73.6 mg PS were dissolved in 1 ml THF.

Absorption cross-section spectra of PtOEP in liquid solutions and of PtOEP doped films are derived from transmission measurements with a commercial spectrophotometer (Beckman type ACTA M IV). The optical constants (absorption coefficient spectrum and refractive index spectrum) of the PtOEP neat film are determined from transmittance and reflectance measurements employing the Fresnel equations for parameter extraction [60,61].

The absolute intrinsic phosphorescence quantum distributions, $E_P(\lambda)$, are determined with a self-assembled fluorimeter in front-face collection arrangement [62,63] (for the definition of intrinsic luminescence quantum distribution see [64]). A scheme of the experimental setup is shown in Fig. 2a. The samples are excited with a tungsten lamp.

The excitation wavelengths, λ_{exc}, were selected with interference filters. In all cases, the excitation intensity for fluorescence quantum yield measurement was less than 0.01 W cm^{-2}. The samples were excited under magic angle conditions (polarizer in excitation path in vertical direction, polarizer in luminescence path oriented under an angle of 54.7° to the vertical). For absolute calibration the dyes quinine sulphate dehydrate (from Aldrich) dissolved in 1 normal aqueous H_2SO_4 ($\lambda_{exc} = 365$ nm, fluorescence quantum yield $\phi_F(C) = 0.546/[1 + 14.5C]$, where C is the dye concentration in mol dm^{-3} [65]), rhodamine 6G in methanol ($\lambda_{exc} = 500$ nm, $\phi_F = 0.94$ [66]), rhodamine 101 in ethanol ($\lambda_{exc} = 530$ nm, $\phi_F = 1.0$ [65]), and cresyl violet in methanol ($\lambda_{exc} = 546$ nm, $\phi_F = 0.54$ [67,68]) are used as reference. The phosphorescence quantum yield is given by $\phi_P = \int E_P(\lambda)\,d\lambda$. The luminescence efficiency of PtOEP in the liquid solutions was determined under air saturated conditions as delivered and after de-aeration by bubbling for 2 h with purified nitrogen (nitrogen of 99.999% purity was passed through an Oxysorb cartridge from Air Liquide to reduce the oxygen content to less than 5 ppb). The phosphorescence quantum yield of the PtOEP doped films and of the neat PtOEP film were measured under ambient atmospheric conditions and in vacuum (pressure 2×10^{-8} bar $= 2 \times 10^{-3}$ Pa).

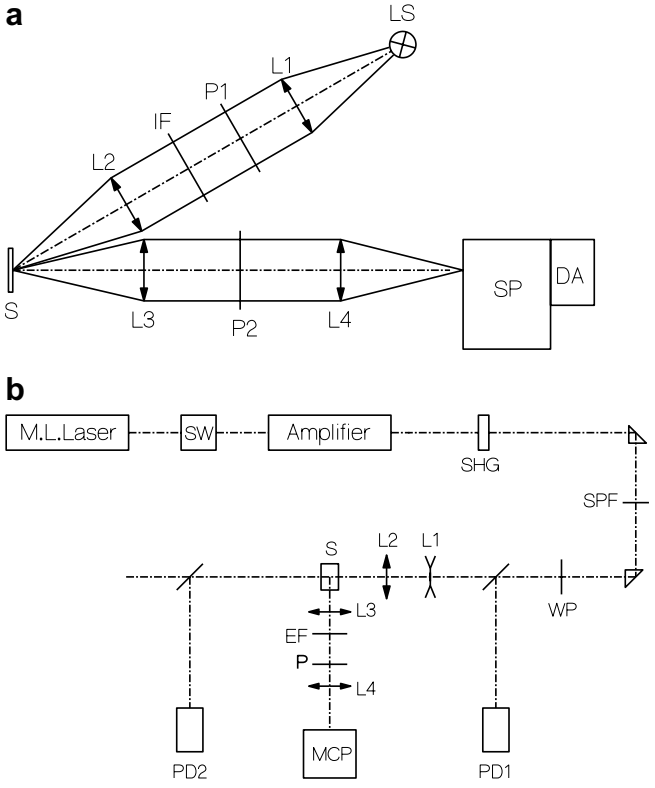

Fig. 2. (a) Experimental setup for phosphorescence quantum distribution determination. LS, tungsten lamp; L1–L4 lenses; IF, interference filter; P1,P2, linear, dichroitic polarizer sheets; S, sample; SP, spectrometer; DA, silicon diode-array detection system. (b) Experimental setup for luminescence lifetime measurement. M.L. Laser, active and passive mode-locked ruby laser; SW, Pockels cell single pulse selector; Amplifier, ruby laser amplifier; SHG, KDP* crystal for second harmonic generation; SPF, short pass filter (subtractive four-prism arrangement with slit for fundamental laser light blocking). WP, half-wave plate for 90° polarization rotation; L1,L2, beam expanding telescope; L3,L4, luminescence collecting lenses; S, sample; EF, long-pass edge filter ($\lambda > 590$ nm); PD1, PD2, photodetectors; MCP, micro-channel-plate photomultiplier.

The temporal luminescence behaviour, $S_P(t)$, was studied by picosecond laser pulse excitation using a mode-locked and frequency doubled ruby laser system (wavelength $\lambda_L = 347.15$ nm, duration $\Delta t_L = 35$ ps) [69] and emission detection with a fast micro-channel-plate photomultiplier (Hamamatsu type R1564U-01) and a fast real-time digital oscilloscope (LeCroy type 9362). The experimental setup is sketched in Fig. 2b. For the air-saturated liquid samples, after subtraction of some solvent contribution, single-exponential phosphorescence decay was observed. The phosphorescence lifetime (triplet-state lifetime), τ_P, is obtained by fitting the function,

$$S_P(t) = S_{P,0} \exp(-t/\tau_P), \tag{1}$$

to the phosphorescence signal trace. The lifetime is determined by oxygen quenching (see below). For the de-aerated liquid solutions and the solid films, after subtraction of some solvent or substrate contribution, non-exponential luminescence signal decay was observed because of triplet–triplet annihilation at finite excitation intensity. The intrinsic $1/e$ phosphorescence lifetime at infinitely low excitation intensity (picosecond laser pulse energy density $w_L \to 0$ leading to negligible triplet population), τ_P, will be extracted below by simulation of the annihilation dynamics.

The radiative lifetime of the T_1–S_0 emission is determined by

$$\tau_{rad,P} = \frac{\tau_P}{\phi_P}. \tag{2}$$

The stimulated emission cross-section spectrum, $\sigma_{em,P}$, is determined from the radiative lifetime, $\tau_{rad,P}$, and the phosphorescence quantum distribution, $E_P(\lambda)$, by [70,71]

$$\sigma_{em,P}(\lambda) = \frac{\lambda^4}{8\pi n_P^2 c_0 \tau_{rad,P}} \frac{E_P(\lambda)}{\int_{em} E_P(\lambda')\,d\lambda'}, \tag{3}$$

where n_P is the mean refractive index in the phosphorescence region, and c_0 is the vacuum light velocity. The integral extends over the phosphorescence emission region em.

The radiative lifetime, $\tau_{rad,P}$, is related to the absorption strength of the relevant transition by the Strickler–Berg formula [72,73]

$$\tau_{rad,P}^{-1} = \frac{g_A}{g_P} \frac{8\pi c_0 n_P^3}{n_A} \frac{\int_{em} E_P(\lambda)\,d\lambda}{\int_{em} E_P(\lambda)\lambda^3\,d\lambda} \int_{abs} \frac{\sigma_{a,P}(\lambda)}{\lambda}\,d\lambda, \tag{4}$$

where g_A is the statistical weight of the singlet ground-state ($g_A = 1$), and g_P is the statistical weight of the triplet state T_1 ($g_P = 3$). n_A is the mean refractive index in the S_0–T_1 absorption region. $\sigma_{a,P}(\lambda)$ is the absorption cross-section of the S_0–T_1 transition. The absorption integral extends over the S_0–T_1 absorption region abs. Eq. (4) will be used

below to separate out the absorption cross-section spectrum of the lowest singlet–triplet transition (responsible for phosphorescence emission) from the complete absorption cross-section spectrum with the aid of the mirror symmetry relation between absorption and emission of a vibronic transition [74].

3. Results

In Fig. 3a, the absorption cross-section spectra of PtOEP dissolved in THF, toluene, and chloroform are shown. The spectra in the three solvents are quite similar. The small peak at 640 nm and the shoulder at 587 nm are attributed to the pure electronic $S_0(0)$–$T_1(0)$ and the first vibronic $S_0(0)$–$T_1(1)$ ground-state singlet to lowest triplet-state transition, respectively. The numbers 0 and 1 in the parentheses denote the vibrational quantum numbers. The singlet–singlet absorption peaks are classified as Q(0), Q(1), B(0), B(1), N, and L [35,75,76]. The B band is called the Soret band. The absorption peak of Q(0) is located at 533 nm, and the absorption peak of B(0) is at 380 nm.

The absorbance spectra of the applied films with 4 wt% and 8 wt% PtOEP in polystyrene, and 8.4 wt% PtOEP in CBP are displayed in Fig. 3b. For the PtOEP doped polystyrene films the Q(0) absorption peak is at 534 nm, and for the PtOEP doped CBP film it is at 538 nm. The absorption cross-section spectra of the film materials polystyrene and CBP are included in Fig. 3a.

The absorption coefficient spectrum, $\alpha(\lambda)$, and the refractive index spectrum, $n(\lambda)$, of the 64.6 nm thick neat film of PtOEP on a quartz glass substrate is shown in Fig. 4. The α and n values are determined by nearly normal incidence transmittance and reflectance measurements and Fresnel equation data analysis [60,61]. The α and n spectra are governed by the Q-band and the Soret band transitions. The weak long-wavelength absorption around 580–640 nm is probably due to some aggregate absorption [33,46,47].

The effective absorption cross-section spectrum, $\sigma_a = \alpha/N$ (N number density of PtOEP molecules), of the neat film is included in Fig. 3a. Since N is not accurately known, it is calibrated to the THF solution spectrum by equating the absorption cross-section integrals for $335\text{ nm} \leqslant \lambda \leqslant 600$ nm, i.e. $\sigma_{a,f}(v) = \left[\alpha_f(v)/\int \alpha_f(v)\,dv\right] \int \sigma_{a,THF}(v)\,dv$, where $v = c_0/\lambda$ is the frequency, and the index f stands for film. The neat film spectrum is somewhat flattened compared to the solution spectra. The Q peak is shifted 13 nm to the red and the B peak is shifted 5 nm to the blue.

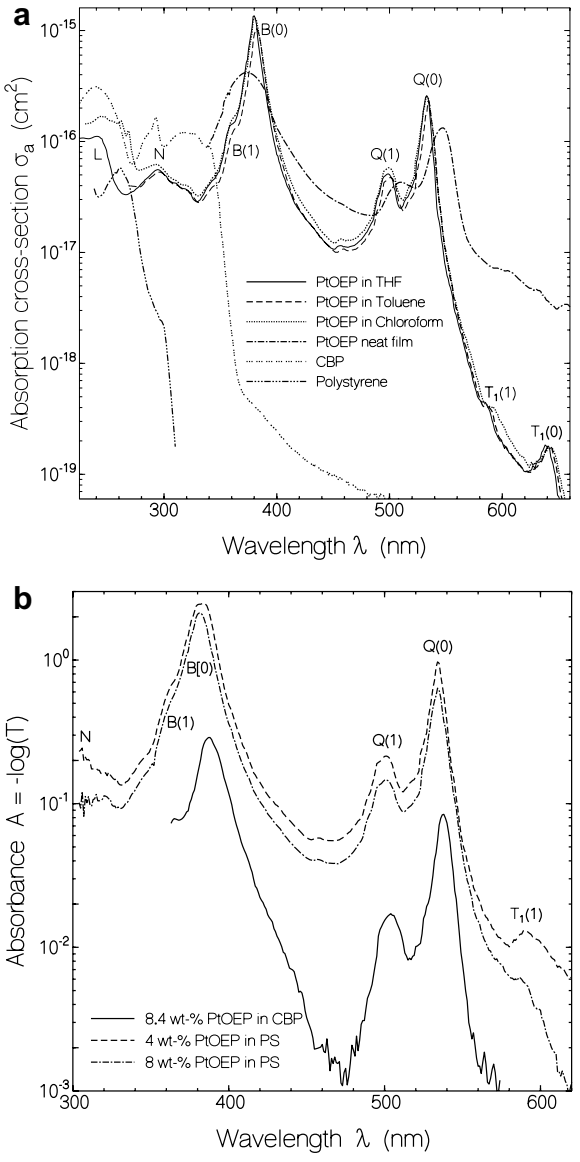

Fig. 3. (a) Absorption cross-section spectra, $\sigma_a(\lambda)$, of PtOEP in THF, toluene, chloroform, and of neat film. Absorption cross-section spectra of polystyrene (from [74]) and of CBP (from [74]) are included. (b) Absorbance spectra, $A(\lambda)$, of applied films of PtOEP doped in CBP and polystyrene.

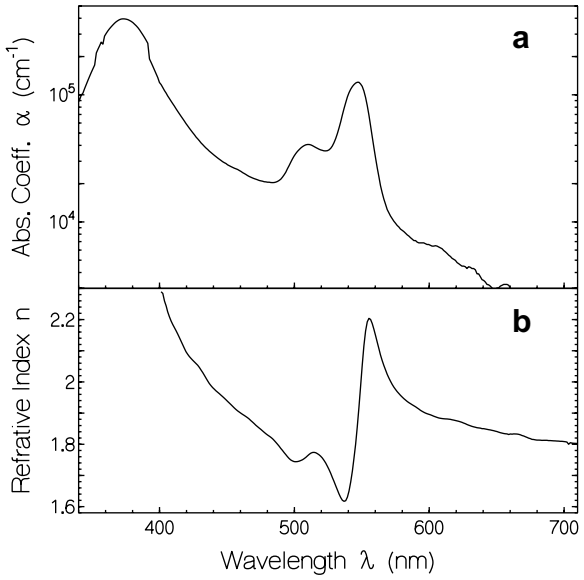

Fig. 4. Absorption coefficient spectrum, $\alpha(\lambda)$, and refractive index spectrum, $n(\lambda)$, of PtOEP neat film on quartz glass substrate. Film thickness, $d_f = 64.6 \pm 2$ nm.

The determined phosphorescence quantum distributions of PtOEP in the as-delivered solvents THF (concentration $C = 8.2 \times 10^{-5}$ mol dm^{-3}), toluene ($C = 8.9 \times 10^{-5}$ mol dm^{-3}), and chloroform ($C = 7 \times 10^{-5}$ mol dm^{-3}), and their de-aerated counterparts are shown in Fig. 5a. The spectral shapes are nearly independent of the solvent. Some vibronic structure is resolved. The phosphorescence quantum yield of the air-saturated samples is rather low in the 0.1% region. This small quantum yield is caused by oxygen quenching. De-aeration increases the phosphorescence efficiency approximately a factor of 300 and brings the phosphorescence quantum yield up to about 40%. The determined phosphorescence quantum yields, $\phi_P = \int E_P(\lambda)\,d\lambda$, are listed in Table 1.

In Fig. 5b the phosphorescence quantum distributions of PtOEP in the solid hosts polystyrene (1 wt%, 4 wt%, 8 wt%), and CBP (8.4 wt%) under ambient conditions are displayed. The obtained phosphorescence quantum yields, ϕ_P, are listed in Table 2. The highest phosphorescence quantum yield under ambient conditions was obtained for PtOEP in CBP ($\phi_P \approx 0.37$) . For PtOEP in polystyrene under ambient conditions the luminescence quantum efficiency is about a factor of two lower. The smaller phosphorescence in polystyrene compared to CBP is due to a higher oxygen permeability of polystyrene compared to CBP. For the highest concentration of 8 wt% PtOEP in polystyrene a slight reduction of phosphorescence efficiency is already observed indicating the onset of PtOEP self-quenching. Bringing a 5 wt% PtOEP doped polystyrene film into vacuum (2×10^{-5} mbar), the phosphorescence quantum yield rose from $\phi_P \approx 0.20$ to $\phi_P \approx 0.54$. Placing the PtOEP doped CBP film into vacuum did not change the phosphorescence quantum yield.

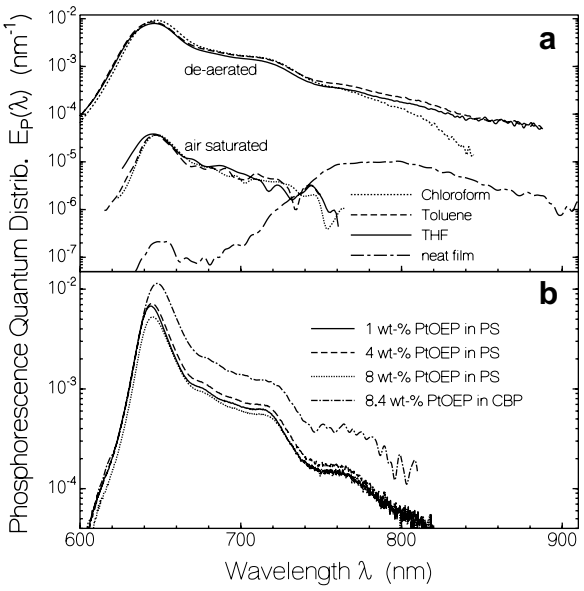

Fig. 5. Phosphorescence quantum distributions of PtOEP. (a) Liquid solutions and neat film. Luminescence passed through a 590 nm long-pass edge filter. Lower curves: air-saturated solutions. Excitation wavelength $\lambda_{exc} = 500$ nm. Cell thickness, $\ell = 1$ mm. Sample transmissions: T_{exc}(THF) = 0.745, T_{exc}(toluene) = 0.652, T_{exc}(chloroform) = 0.393. Upper curves: de-aerated solutions. Excitation wavelength, $\lambda_{exc} = 526$ nm. Cell thickness, $\ell = 1$ cm. Sample transmissions: T_{exc}(THF) = 0.23, T_{exc}(toluene) = 0.27, T_{exc}(chloroform) = 0.24. Dash-dotted line: PtOEP neat film on glass plate; $\lambda_{exc} = 546$ nm. (b) Solid films on glass plates. Host materials are polystyrene and CBP. Excitation wavelengths $\lambda_{exc} = 365$ nm. Sample transmissions: T_{exc}(PS, 1 wt%) = 0.124, T_{exc}(PS, 4 wt%) = 0.125, T_{exc}(PS, 8 wt%) = 0.275, and T_{exc}(CBP, 8.4 wt%) = 0.812. Curves measured under ambient air conditions.

The phosphorescence spectrum of the investigated PtOEP neat film under ambient conditions is included in Fig. 5a. There self-quenching occurs. The phosphorescence quantum efficiency is $\phi_P \approx 0.001$. In vacuum the quantum efficiency increased to $\phi_P \approx 0.0013$. In the neat film the emission spectrum has a different shape: the emission at 650 nm is very small, the main emission occurs in the range from 750 nm to 830 nm. This spectral red shift has been observed in [33,46,47] and has been attributed to PtOEP aggregation [46] with dimeric triplet exciton emission [33,47]. A red-shifted aggregate luminescence was also observed in a mixture of THF with water [46], and it was observed at 10 K in a 5 wt% PtOEP doped TPD thin film (unpublished results from T.T.). Phosphorescent excimer emission is also present in other Pt complexes [48–51] and has been applied for white OLED (WOLED) technology [48–50].

Phosphorescence signal decay curves of PtOEP in liquid solution are displayed in Fig. 6. In the air saturated liquid solutions (Fig. 6a, b, c) single-exponential phosphorescence decays are observed. The phosphorescence lifetimes are in range of 220–290 ns. They are determined by oxygen quenching. In the de-aerated samples (Fig. 6d–f) the phosphorescence lifetime is strongly enlarged. The luminescence signal dropping to $1/e$ of its maximum signal in a time, $\tau_{P,1/e}$, depends on the excitation laser pulse energy density ($\tau_{P,1/e}$ in the 10–30 μs range for the displayed traces with excitation energy densities in the range of 0.2–0.8 mW cm^{-2}). The luminescence decay is non-exponential. At the beginning the decrease is faster than at later times. This behaviour is thought to be due to triplet–triplet annihilation [40,77]. It will be analyzed below. The luminescence decay at longer times becomes exponential (time constant τ_P). It is determined by spontaneous T_1–S_0 triplet–singlet emission and non-radiative T_1–S_0 triplet–singlet intersystem crossing. This phosphorescence lifetime, τ_P, of PtOEP in the studied liquid solutions is of the order of 50 μs. Radiative phosphorescence lifetimes of $\tau_{rad,P} = \tau_P/\phi_P \approx 120$ μs are estimated. The values are listed in Table 1.

The phosphorescence signal decay of 5 wt% PtOEP in polystyrene is shown Fig. 7a and b. Part (a) belongs to ambient (air-saturated) conditions, and part (b) belongs to vacuum (de-aerated) conditions. At the applied energy density of $w_{0L} = 1.7$ mW cm^{-2} (excitation wavelength $\lambda_L = 347.15$ nm) the luminescence decay is non-exponential. The $1/e$ decay time at the beginning was found to be $\tau_{P,1/e}$(ambient) $\approx 10 \pm 1$ μs and $\tau_{P,1/e}$(vacuum) $\approx 11.5 \pm 1$ μs. At later times the decay is approximately exponential

Table 1
Spectroscopic parameters of PtOEP solutions in organic solvents under air-saturated and de-aerated conditions at room temperature

Parameter	THF as-delivered	THF de-aerated	Toluene as-delivered	Toluene de-aerated	Chloroform as-delivered	Chloroform de-aerated
C (mol dm^{-3})	1.8×10^{-4}	4.5×10^{-5}	2.1×10^{-4}	7.7×10^{-5}	2.7×10^{-4}	3.25×10^{-5}
d_s (nm)	21	33	20	28	18.3	37
η (Pa s)	4.8×10^{-4}	4.8×10^{-4}	5.85×10^{-4}	5.85×10^{-4}	5.42×10^{-4}	5.42×10^{-4}
ℓ_d (nm)	21.8	327	19.7	296	23.3	308
ϕ_P	$(1.4\pm0.2)\times10^{-3}$	0.375 ± 0.02	$(1.25\pm0.1)\times10^{-3}$	0.415 ± 0.02	$(1.25\pm0.1)\times10^{-3}$	0.415 ± 0.02
n_A	1.4118	1.4118	1.5104	1.5104	1.4522	1.4522
n_P	1.4074	1.4074	1.5016	1.5016	1.4476	1.4476
τ_P (μs)	0.222 ± 0.02	50 ± 20	0.222 ± 0.02	50 ± 20	0.286 ± 0.02	50 ± 20
$\tau_{rad,P}$ (μs)		≈135		≈120		≈120
$k_{ISC,T_1-S_0}(s^{-1})$		$\approx1.3\times10^4$		$\approx1.2\times10^4$		$\approx1.2\times10^4$
$k_q[O_2]$ (s^{-1})	$\approx4.5\times10^6$		$\approx4.5\times10^6$		3.5×10^6	
k_{TT} (cm^3 s^{-1})		$(5.4\pm2)\times10^{-10}$		$(1.6\pm0.8)\times10^{-10}$		$(2.2\pm0.7)\times10^{-10}$

Table 2
Spectroscopic parameters of PtOEP neat film and in solid matrix at room temperature

Parameter	Neat film	CBP	PS	PS	PS	PS	PS
Condition	In air	In air	In air	In air	In air	In air	In vacuum
Concentration		8.4 wt%	1 wt%	4 wt%	8 wt%	5 wt%	5 wt%
N_0 (cm^{-3})	9.5×10^{20}	$\approx7.3\times10^{19}$	8.7×10^{18}	3.5×10^{19}	6.9×10^{19}	4.4×10^{19}	4.4×10^{19}
d_s (nm)	1.02	2.40	4.86	3.06	2.44	2.83	2.83
R_0 (nm)	0.35	1.4	1.4	1.4	1.4	1.4	1.65
ϕ_{ET}	0.0016	0.038	0.0006	0.009	0.035	0.015	0.038
ϕ_P	0.001 ± 0.0002	0.37 ± 0.04	0.195 ± 0.02	0.215 ± 0.02	0.164 ± 0.02	0.20 ± 0.02	0.54 ± 0.04
n_A	1.88	1.793	1.59	1.59	1.59	1.59	1.59
n_P	1.83	1.792	1.59	1.59	1.59	1.59	1.59
d_f (μm)	0.065	0.27	≈1	1.11	0.36	0.22	0.22
τ_P (μs)	≈0.10	≈30	≈25	≈25	≈25	≈25	≈60
$\tau_{rad,P}$ (μs)	≈100	≈85	≈130	≈120	≈150	≈120	≈120
k_{ISC,T_1-S_0}(s^{-1})		$\approx2.1\times10^4$				$\approx8.3\times10^3$	$\approx8.3\times10^3$
$k_q[O_2]$ (s^{-1})						$\approx3.2\times10^4$	
k_{TT} (cm^3 s^{-1})	$\approx8\times10^{-15}$[a]	$\approx1.2\times10^{-13}$				$\approx6.7\times10^{-14}$	$\approx1\times10^{-13}$

[a] Triplet–triplet annihilation constant for dimeric triplet excitons taken from [47].

with decay times τ_P(ambient) ≈ 20 μs and τ_P(vacuum) ≈ 60 μs. The enhanced initial decay is thought to be due to triplet–triplet annihilation. At long times the phosphorescence decay changes to exponential decay due to radiative triplet–singlet emission and non-radiative triplet–singlet intersystem-crossing.

The luminescence signal decay of 8.4 wt% PtOEP in CBP under vacuum condition is shown in Fig. 7c (there was observed no difference between vacuum conditions and ambient air conditions). At the applied energy density of $w_{0L} = 240$ μW cm^{-2} (excitation wavelength $\lambda_L = 347.15$ nm) the luminescence decay is non-exponential. The $1/e$ decay time at the beginning was found to be $\tau_{P,1/e} \approx 16.5\pm1.5$ μs. At an excitation energy density of $w_{0L} = 85$ μW cm^{-2} the $1/e$ decay time was found to be $\tau_{P,1/e} \approx 30\pm5$ μs, and could be fitted reasonably with a single-exponential function (curves not shown). The enhanced initial decay at higher excitation energy density is thought to be due to triplet–triplet annihilation.

The luminescence decay of the PtOEP neat film is shown in Fig. 7d. The measurement is not very accurate because of strong self-quenching and the occurrence of disturbing short-time emission of the quartz glass substrate which is subtracted in Fig. 7d. A phosphorescence decay time of $\tau_P \approx 150\pm50$ ns is extracted from the displayed signal in Fig. 7d. From the luminescence quantum yield measurements a similar phosphorescence lifetime of $\tau_P = \phi_P\tau_{rad,P} \approx$ 100 ns is obtained ($\phi_P \approx 0.001$, $\tau_{rad,P} \approx$ 100 μs).

In Fig. 8 the stimulated emission cross-section spectra of PtOEP in THF and of 4 wt% PtOEP in polystyrene are shown together with the long-wavelength absorption cross-section of PtOEP in THF. The stimulated emission spectra are calculated by use of Eq. (3) from the phosphorescence quantum distributions and a radiative phosphorescence lifetime of $\tau_{rad,P} = 120$ μs. These stimulated emission cross-section spectra are due to the T_1–S_0 transition. For 4 wt% PtOEP in polystyrene the corresponding S_0–T_1 absorption cross-section spectrum is included in the Fig. 8. It is calculated by use of Eq. (4) (determination of $\int[\sigma_{a,P}(\lambda)/\lambda]\,d\lambda$) assuming mirror symmetry to the T_1–S_0 emission spectrum with image plane at $\lambda_0 = 642$ nm, i.e. $\sigma_{a,P}(\lambda_0-\delta\lambda) \approx (g_P/g_A)\lambda_0[\sigma_{em,P}(\lambda_0+\delta\lambda)/\int\sigma_{em,P}(\lambda)d\lambda]\int[\sigma_{a,P}(\lambda)/\lambda]d\lambda$. The S_0–T_1 absorption cross-section integral is roughly a factor of three larger than the T_1–S_0 stimulated emission cross-section integral because of the threefold triplet degeneracy (statistical weight $g_P = 3$) [73].

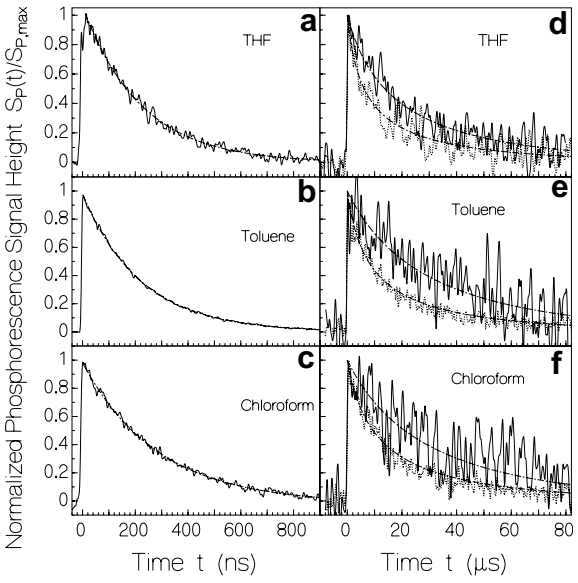

Fig. 6. Temporal phosphorescence signal traces of PtOEP in as-delivered liquid solutions (a–c) and in de-aerated liquid solutions (d–f). Excitation wavelength $\lambda_{exc} = 347.15$ nm. Excitation pulse duration $\Delta t_L = 35$ ps. Dash-dotted curves in (a,b,c) are single-exponential decay fits, and in (d–f) they are triplet–triplet annihilation fits. (a) THF: Concentration $C = 3.4 \times 10^{-5}$ mol dm^{-3}, excitation energy density $w_{0L} = 5.8 \times 10^{-3}$ J cm^{-2} (peak intensity $I_{0L} \approx w_{0L}/\Delta t_L \approx 1.7 \times 10^8$ W cm^{-2}), phosphorescence lifetime fit $\tau_P = 222$ ns. (b) Toluene: $C = 4.2 \times 10^{-5}$ mol dm^{-3}, $w_{0L} = 5 \times 10^{-3}$ J cm^{-2} ($I_{0L} \approx 1.4 \times 10^8$ W cm^{-2}), $\tau_P = 222$ ns. (c) Chloroform: $C = 3.4 \times 10^{-5}$ mol dm^{-3}, $w_{0L} = 4.2 \times 10^{-3}$ J cm^{-2} ($I_{0L} \approx 1.2 \times 10^8$ W cm^{-2}), $\tau_P = 286$ ns. (d) THF: $C = 4.8 \times 10^{-5}$ mol dm^{-3} ($N_0 = 2.7 \times 10^{16}$ cm^2). Solid curve: peak excitation energy density $w_{0L} = 2.4 \times 10^{-4}$ J cm^{-2} ($I_{0L} \approx 7 \times 10^6$ W cm^{-2}, $N_{T,ini,0} \approx 5.7 \times 10^{14}$ cm^{-3}, see Eq. (11)), fitted with annihilation parameter $K_{T,0} = 1 \times 10^5$ s^{-1} and phosphorescence lifetime $\tau_P = 50$ μs. Dotted curve: $w_{0L} = 3.7 \times 10^{-4}$ J cm^{-2} ($I_{0L} \approx 1 \times 10^7$ W cm^{-2}, $N_{T,ini,0} \approx 8.9 \times 10^{14}$ cm^{-3}), fitted with $K_{T,0} = 3.2 \times 10^5$ s^{-1} and $\tau_P = 50$ μs. (e) Toluene. $C = 7.7 \times 10^{-5}$ mol dm^{-3} ($N_0 = 4.6 \times 10^{16}$ cm^2). Solid curve: $w_{0L} = 2.2 \times 10^{-4}$ J cm^{-2} ($I_{0L} \approx 6.3 \times 10^6$ W cm^{-2}, $N_{T,ini,0} \approx 9 \times 10^{14}$ cm^{-3}), fitted with $K_{T,0} = 4 \times 10^4$ s^{-1}, $\tau_P = 50$ μs. Dotted curve: $w_{0L} = 5 \times 10^{-4}$ J cm^{-2} ($I_{0L} \approx 1.4 \times 10^7$ W cm^{-2}, $N_{T,ini,0} \approx 2 \times 10^{15}$ cm^{-3}), fitted with $K_{T,0} = 2.4 \times 10^5$ s^{-1} and $\tau_P = 50$ μs. (f) Chloroform: $C = 3.3 \times 10^{-5}$ mol dm^{-3} ($N_0 = 1.96 \times 10^{16}$ cm^2). Solid curve: $w_{0L} = 2.8 \times 10^{-4}$ J cm^{-2} ($I_{0L} \approx 8 \times 10^6$ W cm^{-2}, $N_{T,ini,0} \approx 4.9 \times 10^{14}$ cm^{-3}), $K_{T,0} = 4 \times 10^4$ s^{-1}, $\tau_P = 50$ μs. Dotted curve: $w_{0L} = 7.3 \times 10^{-4}$ J cm^{-2} ($I_{0L} \approx 2.1 \times 10^7$ W cm^{-2}, $N_{T,ini,0} \approx 1.3 \times 10^{15}$ cm^{-3}), $K_{T,0} = 1.8 \times 10^5$ s^{-1} and $\tau_P = 50$ μs.

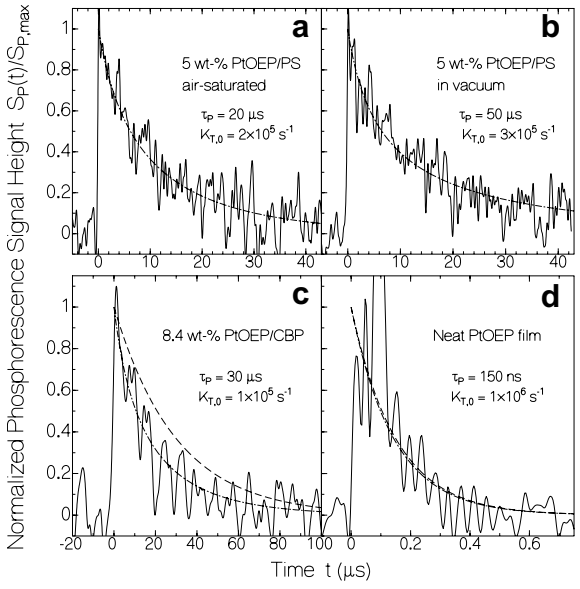

Fig. 7. Phosphorescence signal traces of PtOEP in solid films. Excitation wavelength $\lambda_L = 347.15$ nm. Excitation pulse duration $\Delta t_L = 35$ ps. Dash-dotted curves are triplet–triplet annihilation fits. (a) 5 wt% PtOEP in polystyrene. Film under ambient conditions. Peak excitation energy densities $w_{0L} = 1.7 \times 10^{-3}$ J cm^{-2} ($I_{0L} \approx 5 \times 10^7$ W cm^{-2}, $\Delta t_L = 35$ ps, $\lambda_L = 347.15$ nm, $\sigma_{a,L} = 4.7 \times 10^{-17}$ cm^2, $N_{T,ini,0} \approx 6.0 \times 10^{18}$ cm^{-3}). Fit curve belongs to annihilation parameter $K_{T,0} = 2 \times 10^5$ s^{-1} and phosphorescence lifetime $\tau_P = 20$ μs. (b) 5 wt% PtOEP in polystyrene. Film in vacuum. Peak excitation energy densities $w_{0L} = 1.7 \times 10^{-3}$ J cm^{-2} ($I_{0L} \approx 5 \times 10^7$ W cm^{-2}, $N_{T,ini,0} \approx 6.0 \times 10^{18}$ cm^{-3}). Fit curve belongs to annihilation parameter $K_{T,0} = 3 \times 10^5$ s^{-1} and phosphorescence lifetime $\tau_P = 50$ μs. (c) 8.4 wt% PtOEP in CBP, $w_{0L} \approx 2.41 \times 10^{-4}$ J cm^{-2} ($N_{T,ini,0} \approx 1.6 \times 10^{18}$ cm^{-3}). Dash-dotted curve is fit with $K_{T,0} = 1 \times 10^5$ s^{-1} ($k_{TT} = 1.2 \times 10^{-13}$ cm^3 s^{-1}) and $\tau_P = 30$ μs. Dashed curve is calculated for $K_{T,0} = 0$ and $\tau_P = 30$ μs (d) Neat PtOEP film. Signal is detected in long-wavelength region, $\lambda > 710$ nm (long-pass edge filter in), where dimeric triplet excitons emit. $w_{0L} \approx 1 \times 10^{-3}$ J cm^{-2} ($I_{0L} \approx 4 \times 10^8$ W cm^{-2}, $\Delta t_L = 2.5$ ps, $\lambda_L = 400$ nm, $\sigma_{a,L} = 1.32 \times 10^{-16}$ cm^2, $N_{T,ini,0} \approx 2.6 \times 10^{20}$ cm^{-3}). Dash-dotted curve is fit with $K_{T,0} = 1 \times 10^6$ s^{-1} ($k_{TT} = 8 \times 10^{-15}$ cm^3 s^{-1}, from [47]) and $\tau_P = 150$ ns. Dashed curve is single-exponential fit with $\tau_P = 150$ ns ($K_{T,0} = 0$).

4. Discussion

4.1. Fluorescence situation

In the luminescence spectra measurements the emission is passed through a 590 nm long-pass edge filter with the exception of the PtOEP doped films, where the luminescence was excited at 365 nm and the emission signal was passed through a 400 nm long-pass edge-filter (filtering out of Rayleigh scattered excitation light). In these measurements with a signal to noise ratio of 1000:1 no fluorescence signal could be resolved which should appear at around 540 nm slightly red-shifted to the Q(0) absorption peak (first excited singlet state S_1). Our signal to noise ratio was not high enough to resolve a fluorescence signal out of the background level. In [31] a S_1 state lifetime of $\tau_F < 15$ ps was determined. Application of Eq. (4) to the S_0–S_1 absorption band (Fig. 3, upper wavelength limit $\lambda_u \approx 470$ nm) gives a S_1 state radiative lifetime of $\tau_{rad,F} \approx 24$ ns, and the fluorescence quantum is estimated to be $\phi_F = \tau_F/\tau_{rad,F} < 6 \times 10^{-4}$. The short fluorescence lifetime is caused by S_1–T_1 intersystem-crossing (rate $k_{ISC,S1\text{-}T1} \approx \tau_F^{-1} > 7 \times 10^{10}$ s^{-1}). Compared to the S_1–T_1 intersystem crossing rate the S_1–S_0 internal conversion rate, k_{IC}, is thought to be negligible (quantum yield of internal conversion $\phi_{IC} = k_{IC}\tau_F$ is negligible). The quantum yield of triplet formation, $\phi_T = 1 - \phi_F - \phi_{IC}$, is nearly 100%. In [33] a weak luminescence was observed around 550 nm for a PtOEP neat film and a film consisting of 6 wt% PtOEP, 75 wt% TPD (*N*,*N*′-diphenyl-*N*,*N*′-bis(3-methylphenyl)-1,1′-biphenyl-4,4′ diamine), and 19 wt% PC (bisphenol-A-polycarbonate) and it was identified as hot Q-band luminescence (Q-band populated from lower lying triplet state). A weak delayed fluorescence was observed for

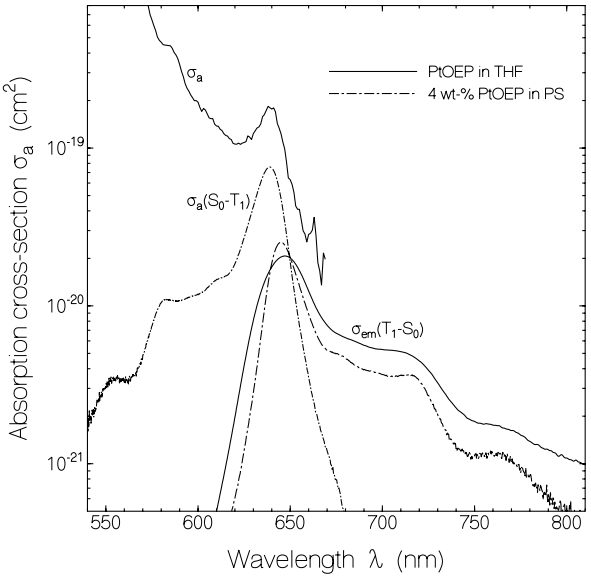

Fig. 8. Triplet–singlet stimulated emission cross-section spectra, $\sigma_{em,P} = \sigma_{em}(T_1\text{–}S_0)$, of PtOEP in THF and of 4 wt% PtOEP in polystyrene, together with absorption cross-section spectra, $\sigma_a(\lambda)$, of PtOEP in THF and $\sigma_{a,P} = \sigma_a(S_0\text{–}T_1)$ of 4 wt% PtOEP in polystyrene.

a PtOEP doped film in [78], where the sample was excited with pulses of a mode-locked Ti:sapphire laser and the emission at a delayed time in the μs range was recorded with an intensified gated diode array detection system coupled to a spectrometer. The delayed fluorescence was identified as hot band emission.

4.2. Radiative lifetime, intersystem-crossing, and oxygen quenching

The Einstein-type calculation of the singlet–triplet absorption from the phosphorescence quantum distribution and phosphorescence lifetime measurements Eqs. (2)–(4) identifies the weak absorption peak at 639 nm as S_0–T_1 transition.

The phosphorescence quantum yield of PtOEP, ϕ_P, is determined by the ratio of the radiative emission rate constant, $k_{rad,P} = \tau_{rad,P}^{-1}$, to the total relaxation rate constant, $k_{tot} = \tau_P^{-1}$, whereby the total rate constant is composed of the radiative rate constant, the intersystem-crossing rate constant, $k_{ISC,T_1\text{–}S_0}$, and the molecular oxygen quenching rate constant, $k_{ox} = k_q[O_2]$ ($[O_2]$ is the concentration of dissolved oxygen). It is given by [79]

$$\phi_P = \frac{k_{rad,P}}{k_{tot}} = \frac{\tau_{rad,P}^{-1}}{\tau_P^{-1}} = \frac{\tau_{rad,P}^{-1}}{\tau_{rad,P}^{-1} + k_{ISC,T_1\text{–}S_0} + k_q[O_2]} = \frac{1}{1 + k_{ISC,T_1\text{–}S_0}\tau_{rad,P} + \tau_{rad,P}k_q[O_2]}. \quad (5)$$

The total relaxation rate is

$$k_{tot} = \tau_P^{-1} \approx \tau_{rad,P}^{-1} + k_{ISC,T_1\text{–}S_0} + k_q[O_2]. \quad (6)$$

The phosphorescence quantum yields of PtOEP in as-delivered liquid tetrahydrofuran (THF), toluene, and chloroform are in the 0.1% region and the picosecond-pulse excited phosphorescence decays single-exponentially with time constants of around 250 ns. The small phosphorescence quantum yields are caused by molecular oxygen phosphorescence quenching. The oxygen quenching rate is $k_q[O_2] \approx \tau_P^{-1} - \tau_{rad,P}^{-1} - k_{ISC,T_1\text{–}T_0} \approx \tau_P^{-1} \approx 4 \times 10^6\ s^{-1}$. Values of $k_q[O_2]$ are included in Table 1.

In the de-aerated liquid solutions the phosphorescence quantum efficiency increased to about 40% and the low-intensity phosphorescence lifetime increased to about 50 μs. A radiative phosphorescence lifetime of $\tau_{rad,P} \approx 120$ μs is determined. The T_1 state relaxation of de-aerated PtOEP solutions is caused by T_1–S_0 radiative emission (spontaneous emission, quantum efficiency $\phi_P \approx 0.4$) and T_1–S_0 intersystem crossing (quantum efficiency, $\phi_{ISC,T_1\text{–}S_0} \approx 1 - \phi_P \approx 0.6$, rate-constant $k_{ISC,T_1\text{–}S_0} \approx \tau_P^{-1} - \tau_{rad,P}^{-1} = \phi_{ISC,T_1\text{–}S_0}\tau_P^{-1} \approx 1.2 \times 10^4\ s^{-1}$ since $[O_2] \approx 0$, see Table 1). The radiative lifetime in different media is thought to be related by the refractive index dependence $\tau_{rad}(n_1)/\tau_{rad}(n_2) = n_2^2/n_1^2$ (n is refractive index).

4.3. Triplet–triplet annihilation and intrinsic phosphorescence lifetime

The phosphorescence decay in the de-aerated samples and in the doped films is influenced by triplet–triplet annihilation after picosecond laser pulse excitation.

The dynamics of triplet–triplet annihilation in organometallic compounds is described in detail in [19] (see also [74]). After picosecond pulse excitation the excited electrons are accumulated in the T_1 triplet state, ^{3}PtOEP. Two nearby excited molecules interact by transferring one molecule to an excited singlet-state, ^{1}PtOEP*, and transferring the other molecule to the singlet ground-state, ^{1}PtOEP. The excited singlet-state molecule relaxes back non-radiatively to the initial triplet-state, ^{3}PtOEP. Thereby one excitation is annihilated. The overall annihilation reaction is

$$^3\text{PtOEP} + {}^3\text{PtOEP} \xrightarrow{k_{TT}} {}^3\text{PtOEP} + {}^1\text{PtOEP}, \quad (7)$$

where k_{TT} is the triplet–triplet annihilation constant. The triplet-state number density, N_T, decays due to radiative and non-radiative triplet–singlet relaxation (triplet-state lifetime τ_T equal to phosphorescence time constant τ_P), and due to triplet–triplet annihilation according to Baldo et al. [19]

$$\frac{dN_T}{dt} = -\frac{N_T}{\tau_T} - \frac{1}{2}k_{TT}N_T^2. \quad (8)$$

The solution of this Riccati differential equation with the initial condition, $N_T(0) = N_{T,ini}$, is [19]

$$N_T(t) = \frac{N_{T,ini}}{(1 + K_T\tau_T)\exp(t/\tau_T) - K_T\tau_T} \quad (9)$$

with

$$K_T = \frac{1}{2} k_{TT} N_{T,int}. \quad (10)$$

The initial triplet population number density, $N_{T,ini}$, is estimated from the pump laser excitation energy density, w_L, by the relation [80]

$$N_{T,ini} = \frac{N_0 w_L / w_s}{1 + w_L / w_s}, \quad (11)$$

where $w_s = h\nu_L/\sigma_{a,L}$ ($\approx$0.011 J cm^{-2} in our case) is the saturation energy density [80], h is the Planck constant, $\nu_L = c_0/\lambda_L$ is the pump laser frequency, $\sigma_{a,L}$ is the absorption cross-section at the laser frequency, and N_0 is the number density of PtOEP molecules. For $w_L < w_s$, Eq. (11) simplifies to

$$N_{T,ini} = \frac{N_0 \sigma_{a,L} w_L}{h\nu_L}, \quad (12)$$

The phosphorescence intensity, $I_P(r, t)$, is proportional to the triplet population, $N_T(r, t)$, i.e. $I_P(r, t) = \kappa N_T(r, t)$, where r is the cross-sectional coordinate, and κ is the proportionality constant. Therefore, the phosphorescence intensity is expected to be [74]

$$I_P(r,t) = \frac{\kappa N_{T,ini}(r)}{[1 + K_T(r)\tau_T]\exp(t/\tau_T) - K_T(r)\tau_T}. \quad (13)$$

Assuming a Gaussian energy density distribution, $w_L(r) = w_{0L}\exp(-r^2/r_{0L}^2)$, the phosphorescence power, $S_P(t)$, is given by

$$S_P(t) = \int_0^\infty \frac{\kappa N_{T,int,0}\exp(-r^2/r_{0L}^2)}{[1 + K_{T,0}\exp(-r^2/r_{0L}^2)\tau_T]\exp(t/\tau_T) - K_{T,0}\exp(-r^2/r_{0L}^2)\tau_T} \times 2\pi r\,dr, \quad (14)$$

and the normalized phosphorescence power, $S_P(t)/S_P(0)$, is

$$S_P(t)/S_P(0) = 2\int_0^\infty \frac{\exp(-r^2)}{[1 + K_{T,0}\exp(-r^2)\tau_T]\exp(t/\tau_T) - K_{T,0}\exp(-r^2)\tau_T} r\,dr, \quad (15)$$

with

$$K_{T,0} = \frac{1}{2} k_{TT} N_{T,ini,0} = \frac{1}{2} k_{TT} \frac{N_0 w_{0L}/w_s}{1 + w_{0L}/w_s}. \quad (16)$$

The non-exponential phosphorescence signal decay curves in Fig. 6d–f (de-aerated solutions) and in Fig. 7a–d are fitted by Eq. (15). The fit parameters, $K_{T,0}$, together with w_{0L}, and $N_{T,ini,0}$ are listed in the figure captions. The obtained triplet–triplet annihilation constants, k_{TT}, are given in Tables 1 and 2. For the de-aerated solutions k_{TT} is in the range of 2×10^{-10}–5×10^{-10} cm^3 s^{-1}. For the PtOEP doped thin films the obtained triplet–triplet annihilation constants are around $k_{TT} \approx 10^{-13}$ cm^3 s^{-1}. In liquid solution the factor of thousand larger triplet–triplet annihilation constant is thought to be due to molecular diffusion of the triplet excited PtOEP molecules (collisional quenching). In the doped films only energy transfer between excited molecules and neighbouring unexcited molecules may bring two excited molecules together for annihilation which are originally separated further apart than necessary for annihilation. For the triplet–triplet annihilation of PtOEP in CBP a value of $k_{TT} = 3\times10^{-14}$ cm^3 s^{-1} was reported in [19]. It is near to our result of $k_{TT} = 1.2\times10^{-13}$ cm^3 s^{-1}. For the neat PtOEP film the triplet–triplet annihilation result of $k_{TT}^D = 8\times10^{-15}$ cm^3 s^{-1} for dimeric triplet excitons from [47] was used in our fit (Fig. 7d, dash-dotted curve) since there is nearly no monomeric triplet–singlet phosphorescence present (see Fig. 5a), and therefore no monomeric triplet–triplet annihilation can be observed. In the experiments (Fig. 7d) only the dimeric triplet exciton emission was collected by the applied long-pass edge filter. The influence of triplet–triplet annihilation is negligible and not resolvable in our experiments, as seen by the dashed curve which was calculated for $k_{TT} = 0$.

In the liquid solutions the diffusion length, ℓ_d, within the phosphorescence lifetime is given by the Einstein–Smoluchowski relation [81]

$$\ell_d = \left(\frac{k_B\vartheta}{2\pi\eta r}\tau_P\right)^{1/2}, \quad (17)$$

where k_B is the Boltzmann constant, ϑ is the temperature, η is the dynamic viscosity, and r is the molecule radius ($r = [3V_m/(4\pi)]^{1/3}$, molecular volume $V_m = M_m/(\rho N_A)$, with M_m the molar mass, ρ the density, and N_A the Avogadro constant). A PtOEP radius of $r \approx 0.63$ nm is obtained. Calculated diffusion lengths are included in Table 1. The PtOEP molecular separation is $d_s \approx N_0^{1/3} = (CN_A/1000)^{1/3}$, where N_0 is the PtOEP number density, and C is the PtOEP concentration in mol dm^{-3}. Calculated separation distances are included in Tables 1 and 2. For the de-aerated solutions the diffusion length is considerably longer than the separation distance.

The efficiency of Förster-type energy transfer is given by [64,82,83]

$$\phi_{ET} = \frac{k_{ET}}{k_{ET} + k_{P,0}} = \frac{1}{1 + \left(\frac{d_s}{R_0}\right)^6}, \quad (18)$$

where $k_{ET} = k_{P,0}(R_0/d_s)^6$ is the rate of energy transfer, $k_{P,0}$ is the rate of triplet-state de-population in the absence of energy transfer, and R_0 is the critical Förster distance, where $k_{ET} = k_{P,0}$. The critical Förster distance is given by [64,83,84]

$$R_0^6 = \frac{9\overline{\kappa^2}}{128\pi^5 n^4}\int E_P(\lambda)\sigma_a(\lambda)\lambda^4\,d\lambda, \quad (19)$$

where n is the average refractive index in the overlap region of absorption and emission, and $\overline{\kappa^2} = 2/3$ is a statistical isotropic orientation factor [64]. Calculated R_0 and ϕ_{ET} values are included in Table 2. Small ϕ_{ET} values indicate small energy-transfer contributions to the triplet–triplet annihilation coefficients, k_{TT}, because of inefficient excitation movement to another excited molecule.

4.4. Situation of amplification of spontaneous emission

In films of fluorescent organic molecules [85,86] and polymers [87] wave-guided amplification of spontaneous emission (travelling-wave lasing) [88] and feed-back laser action [89,90] has been observed (for reviews see [87,91–94]). Here, intense transverse picosecond laser pumping of a 2.7 μm thick film consisting of 4 wt% PtOEP in polystyrene (excitation wavelength $\lambda_L = 347.15$ nm, pulse duration $\Delta t_L = 35$ ps, excitation energy density up to $w_{0L} = 1.8 \times 10^{-2}$ J cm^{-2}, pumped film area 0.2 mm × 5 mm) gave no indication of amplified spontaneous emission which should have shown up in a spectral narrowing of the edge-emitted triplet emission spectrum and a nonlinear increase of the emission signal with excitation intensity (in direction of line focus, where amplification length is longest [88]). As shown in Fig. 9a the spectral shapes are the same at low and high excitation intensity. In Fig. 9b it is seen that the edge-emitted phosphorescence peak, $S_P(\lambda_{max})$, rises linearly with excitation energy density, and levels off at high excitation energy densities. This levelling-off is thought to be due to the occurrence of triplet–triplet annihilation, and due to triplet-state population saturation as the excitation energy density, w_{0L}, approaches the saturation energy density of ground-state depletion, $w_s = h\nu_L/\sigma_{a,L} \approx 1.1 \times 10^{-2}$ J cm^{-2} [80]. The maximum amplification of spontaneous emission, $G(\lambda) = S_{ASE}(\lambda)/S_P(\lambda)$, is approximately given by [88]

$$G(\lambda) = \exp[N_{T,ini,0}\sigma_{em,eff}(\lambda)\ell'] = \exp\left[\frac{N_0 w_{0L}/w_s}{1 + w_{0L}/w_s}\sigma_{em,eff}(\lambda)\ell'\right], \tag{20}$$

where $\sigma_{em,eff}(\lambda) = \sigma_{em}(\lambda) - \sigma_{ex}(\lambda)$ is the effective stimulated emission cross-section, $\sigma_{ex}(\lambda)$ is the excited-state absorption cross-section, and ℓ' is the effective gain length ($\leqslant$ pumped length ℓ because of ground-state re-absorption and scattering losses). Neglecting excited-state absorption, ground-state re-absorption, and scattering losses, a maximum gain factor of $G_{max} \approx 1.25$ is estimated using $w_{0L} = 0.018$ J cm^{-2}, $N_0 \approx 3.5 \times 10^{19}$ cm^{-3}, $w_s = 1.1 \times 10^{-2}$ J cm^{-2}, $\sigma_{em,max} = 2 \times 10^{-20}$ cm^2, and $\ell' = 0.5$ cm. This maximum gain is rather low. The non-observation of any amplification of phosphorescence light indicates that the excited-state absorption is equal or larger than the stimulated emission cross-section and/or the effective gain length is small compared to the pumped sample length. At whatever wavelength, λ, where $\sigma_{ex}(\lambda) > \sigma_{em}(\lambda)$, no light amplification occurs and no laser action is possible.

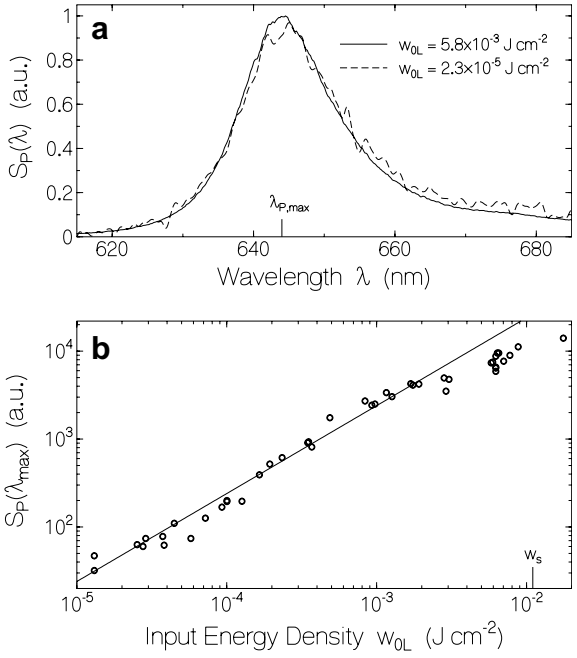

Fig. 9. (a) Edge-emitted spectra from a 4 wt% PtOEP/PS thin film (thickness 2.7 μm) pumped with second harmonic pulses of a mode-locked ruby laser ($\lambda_L = 347.15$ nm, $\Delta t_L \approx 35$ ps). Exposed area is 0.2 mm × 5 mm. Input laser peak energy densities, w_{0L}, are listed in figure. (b) Dependence of spectral signal peak, $S_P(\lambda_{max})$, on input excitation laser peak energy density, w_{0L}. Circles are experimental points. Straight line shows linear relation between signal, $S_P(\lambda_{max})$, and input energy density, w_{0L}, before occurrence of triplet–triplet annihilation and ground-state depletion ($w_{0L} \ll w_s$).

5. Conclusions

In this paper the absorption and emission spectroscopic behaviour of the metal-organic complex PtOEP dissolved in three organic solvents (chloroform, toluene, and tetrahydrofuran), doped in organic films (polystyrene and CBP), and as neat film on a quartz glass plate has been studied. The enhancement of spin–orbit coupling by the heavy metal Pt causes measurable long-wavelength S_0–T_1 singlet–triplet absorption, practically 100% excited-state singlet–triplet intersystem crossing, and high-efficient phosphorescence in doped films and in de-aerated solutions at room temperature. In neat films the phosphorescence quantum yield is reduced to about 0.1% by self-quenching, and the phosphorescence spectrum is red-shifted due to aggregation (dimeric triplet excitons [33,47]). In air-saturated liquid solution molecular oxygen quenching reduces the phosphorescence quantum efficiency to the 0.1% region. Also in the PtOEP doped polystyrene films some oxygen quenching was observed (application as oxygen sensor [32,36–39,41–44]).

The T_1–S_0 stimulated emission cross-section spectrum has been extracted from the phosphorescence quantum distribution and the radiative phosphorescence lifetime. Mirror symmetry arguments between the emission spectrum and the absorption spectrum together with the Einstein coefficient relations between absorption and emission of a transition have been applied to reveal the S_0–T_1 absorption cross-section spectrum peaking at about 639 nm.

Under short-pulse laser excitation conditions in heavily doped films the phosphorescence efficiency is reduced and the phosphorescence lifetime is shortened by triplet–triplet

annihilation. This annihilation may affect the OLED performance in nanosecond pulse applications.

Amplification of spontaneous emission in PtOEP doped films was not achieved at room temperature since the stimulated emission cross-section is small and likely less than the excited-state absorption cross-section. This situation shows that laser action of PtOEP on the T_1–S_0 transition is not possible.

Acknowledgements

We thank the Corporate R&D Laboratories, Pioneer Corporation, Japan for kindly providing the PtOEP neat film evaporated on quartz plate, and we thank Anja Merkel for technical assistance. One of the authors (T.T.) is indebted to the Japan Society for Promotion of Science for a partial support by the Grant-in-Aid for Scientific Research (C, Project No. 15550165).

References

[1] H. Xin, F.Y. Li, M. Guan, C.H. Huang, M. Sun, K.Z. Wang, Y.A. Zhang, L.P. Jin, J. Appl. Phys. 94 (2003) 4729.
[2] S. Hoshino, H. Suzuki, Appl. Phys. Lett. 69 (1996) 224.
[3] Y. Ma, C.-M. Che, H.-Y. Chao, X. Xhou, W.-H. Chau, J. Shen, Adv. Mater. 11 (1989) 852.
[4] M.A. Baldo, M.E. Thompson, S.R. Forrest, Pure Appl. Chem. 71 (1999) 2095.
[5] V. Cleave, G. Yahioglu, P.L. Barny, R.H. Friend, N. Tessler, Adv. Mater. 11 (1999) 285.
[6] R.W.T. Higgins, A.P. Monkman, H.-G. Nothofer, U. Scherf, J. Appl. Phys. 91 (2002) 99.
[7] D.F. O'Brien, C. Giebeler, R.B. Fletcher, A.J. Cadby, L.C. Palilis, D.G. Lidzey, P.A. Lane, D.D.C. Bradley, W. Blau, Synth. Met. 116 (2001) 379.
[8] P.A. Lane, L.C. Palilis, D.F. O'Brien, C. Giebeler, A.J. Cadby, D.G. Lidzey, A.J. Campbell, W. Blau, D.D.C. Bradley, Phys. Rev. B 63 (2001) 235206.
[9] D.F. O'Brien, M.A. Baldo, M.E. Thompson, S.R. Forrest, Appl. Phys. Lett. 74 (1999) 442.
[10] M.A. Baldo, D.F. O'Brien, Y. You, A. Shoustikov, S. Silbey, M.E. Thompson, S.R. Forrest, Nature 395 (1998) 151.
[11] V. Cleave, G. Yahioglu, P.L. Barny, D.-H. Hwang, A.B. Holmes, R.H. Friend, N. Tessler, Adv. Mater. 13 (2001) 44.
[12] M. Cocchi, V. Fattori, D. Virgili, C. Sabatini, P. Di Marco, M. Maestri, J. Kalinowski, Appl. Phys. Lett. 84 (2004) 1052.
[13] C.-L. Lee, K.B. Lee, J.-J. Kim, Mater. Sci. Eng. B85 (2001) 228.
[14] H.-Y. Oh, J.K. Ahn, S.S. Yoon, S. Lee, J.-H. Yang, S.T. Kim, J. Korean Phys. Soc. 39 (2001) S49.
[15] M.A. Baldo, S. Lamansky, P.E. Burrows, M.E. Thompson, S.R. Forrest, Appl. Phys. Lett. 75 (1999) 4.
[16] T. Watanabe, K. Nakamura, S. Kawami, Y. Fukuda, T. Tsuji, T. Wakimoto, S. Miyaguchi, SPIE 4105 (2001) 175.
[17] M.J. Yang, T. Tsutsui, Jpn. J. Appl. Phys., Part 2 39 (8A) (2000) L828.
[18] Y. Kawamura, S. Yanagida, S.R. Forrest, J. Appl. Phys. 92 (2002) 87.
[19] M.A. Baldo, C. Adachi, S.R. Forrest, Phys. Rev. B 62 (2000) 10967.
[20] S. Lamansky, P. Djurovich, D. Murphy, F. Abdel-Razzaq, H.-E. Lee, C. Adachi, P.E. Burrows, S.R. Forrest, M.E. Thompson, J. Am. Chem. Soc. 123 (2001) 4304.
[21] R.R. Das, C.-L. Lee, J.-J. Kim, Mat. Res. Soc. Symp. Proc. 708 (2002) BB3.39.
[22] X. Gong, J.C. Ostrowski, D. Moses, G.C. Guillermo, C. Bazan, A.J. Heeger, Adv. Funct. Mater. 13 (2003) 439.
[23] X. Gong, J.C. Ostrowski, D. Moses, G.C. Guillermo, C. Bazan, A.J. Heeger, J. Polym. Sci. Part B: Polym. Phys. 41 (2003) 2691.
[24] F. Shen, H. Xia, C. Zhang, D. Lin, X. Liu, Y. Ma, Appl. Phys. Lett. 84 (2004) 55.
[25] A. Nakamura, T. Tada, M. Mizukami, S. Yagyu, Appl. Phys. Lett. 84 (2004) 130.
[26] M. Ikai, S. Tokito, Y. Sakamoto, T. Suzuki, Y. Taga, Appl. Phys. Lett. 79 (2001) 156.
[27] M.A. Baldo, M.E. Thompson, S.R. Forrest, Nature 403 (2000) 750.
[28] R.C. Kwong, S. Lamansky, M.E. Thompson, Adv. Mater. 12 (2000) 1134.
[29] C.-L. Lee, K.B. Lee, J.-J. Kim, Appl. Phys. Lett. 77 (2000) 2280.
[30] D. Eastwood, M. Gouterman, J. Mol. Spectrosc. 35 (1970) 359.
[31] G. Ponterini, N. Serpone, M.A. Bergkamp, T.L. Netzel, J. Am. Chem. Soc. 105 (1983) 4639.
[32] D.B. Papkovsky, Sensor. Actuator. B 29 (1995) 213.
[33] J. Kalinowski, W. Stampor, J. Szmytkowski, M. Cocchi, D. Virgili, P. Di Marco, J. Chem. Phys. 122 (2005) 154710.
[34] K. Kalyanasundaram, Photochemistry of Polypyridine and Porphyrin Complexes, Academic Press, New York, 1992.
[35] M. Gouterman, in: D. Dolphin (Ed.), The Porphyrins, Physical Chemistry, Part A, vol. III, Academic Press, New York, 1978, p. 1.
[36] D.B. Papkovsky, J. Ohah, I.V. Mironov, A.I. Yaropolov, A.P. Savitsky, Biosens. Bioelectron. 7 (1991) 199.
[37] K. Eaton, P. Douglas, Sensor. Actuator. B 82 (2002) 94.
[38] Y. Amao, K. Asai, I. Okura, J. Porphyr. Phthalocya. 4 (2000) 292.
[39] A. Mills, A. Lepre, Anal. Chem. 69 (1997) 4653.
[40] N.J. Turro, Modern Molecular Photochemistry, Benjamin/Cummings Publ. Co. Inc., Menlo Park, Ca, 1978 (Chapter 14).
[41] G. Dimarco, M. Lanza, Sensor. Actuator. B 63 (2000) 42.
[42] Y. Amao, K. Asia, T. Miyashita, I. Okura, Polm. Adv. Technol. 11 (2000) 705.
[43] S.-K. Lee, I. Okura, Spectrochim. Acta A 54 (1998) 91.
[44] I. Klimant, M. Kühl, N.R. Glud, G. Holst, Sensor. Actuator. B 38–39 (1997) 29.
[45] S. Grenoble, M. Gouterman, G. Khalil, J. Callis, L. Dalton, J. Lumin. 113 (2005) 33.
[46] T. Dienel, H. Proehl, T. Fritz, K. Leo, J. Lumin. 110 (2004) 253.
[47] J. Mezyk, J. Kalinowski, F. Meinardi, R. Tubino, Appl. Phys. Lett. 86 (2005) 111916.
[48] B.W. D'Andrade, J. Brooks, V. Adamovich, M.E. Thompson, S.R. Forrest, Adv. Mater. 14 (2002) 1032.
[49] V. Adamovich, J. Brooks, A. Tamayo, A.M. Alexander, P.L. Djurovich, B.W. D'Andrade, C. Adachi, S.R. Forrest, M.E. Thompson, New J. Chem. 26 (2002) 1171.
[50] B.W. D'Andrade, S.R. Forrest, Adv. Mater. 16 (2004) 1585.
[51] B. Ma, J. Li, I. Djurovich, M. Yousufuddin, R. Bau, M.E. Thompson, J. Am. Chem. Soc. 127 (2005) 28.
[52] T. Tsuboi, M. Tanigawa, Thin Solid Films 438–439 (2003) 301.
[53] T. Tsuboi, Y. Wasai, N. Nabatova-Gabain, Thin Solid Films 496 (2006) 674.
[54] M.A. Baldo, S.R. Forrest, Phys. Rev. B 62 (2000) 10958.
[55] M.A. Baldo, M. Segal, Phys. Status Solidi A 201 (2004) 1205.
[56] K. Goushi, R. Kwong, J.J. Brown, H. Sasabe, Jpn. J. Appl. Phys. 95 (2004) 1205.
[57] T. Tsuboi, H. Murayama, A. Penzkofer, Appl. Phys. B 81 (2005) 93.
[58] T. Tsuboi, H. Murayama, A. Penzkofer, Thin Solid Films 499 (2006) 306.
[59] G. Ramos-Ortiz, Y. Oki, B. Domercq, B. Kippelen, Phys. Chem. Chem. Phys. 4 (2002) 4109.
[60] A. Penzkofer, E. Drotleff, W. Holzer, Opt. Commun. 158 (1998) 221.
[61] W. Holzer, M. Pichlmaier, A. Penzkofer, D.D.C. Bradley, W.J. Blau, Opt. Commun. 163 (1999) 24.

[62] A. Penzkofer, W. Leupacher, J. Lumin. 37 (1987) 61.
[63] W. Holzer, M. Pichlmaier, A. Penzkofer, D.D.C. Bradley, W.J. Blau, Chem. Phys. 246 (1999) 445.
[64] Th. Förster, Fluoreszenz organischer Verbindungen, Vandenhoeck und Ruprecht, Göttingen, Germany, 1951.
[65] W.H. Melhuish, J. Phys. Chem. 65 (1961) 229.
[66] R. Sens, Dissertation, Universität Gesamthochschule, Siegen, 1994.
[67] D.F. Eaton, EPA Newslett. 28 (1986) 21.
[68] D. Madge, J.H. Brannon, T.L. Cramers, J. Olmsted III, J. Phys. Chem. 84 (1979) 696.
[69] P. Weidner, A. Penzkofer, Opt. Quant. Electron. 25 (1993) 1.
[70] O.G. Peterson, J.P. Webb, W.C. McColgin, J.H. Eberly, J. Appl. Phys. 42 (1971) 1917.
[71] A.V. Deshpande, A. Beidoun, A. Penzkofer, G. Wagenblast, Chem. Phys. 142 (1990) 123.
[72] S.J. Strickler, R.A. Berg, J. Chem. Phys. 37 (1962) 814.
[73] J.B. Birks, D.J. Dyson, Proc. Roy. Soc. London A 275 (1963) 135.
[74] W. Holzer, A. Penzkofer, T. Tsuboi, Chem. Phys. 308 (2005) 93.
[75] J.R. Platt, in: A. Hollaender (Ed.), Visible and Near-visible Light, Radiation Biology, vol. III, McGraw-Hill, New York, 1956, p. 71 (Chapter 2).
[76] H. Gratz, A. Penzkofer, Chem. Phys. 254 (2000) 363.
[77] M. Gouterman, J. Chem. Phys. 30 (1959) 1139.
[78] J.M. Lupton, J. Klein, Chem. Phys. Lett. 363 (2002) 204.
[79] B. Valeur, Molecular Fluorescence. Principles and Applications, Wiley–VCH, Weinheim, 2002.
[80] M. Hercher, Appl. Opt. 6 (1967) 947.
[81] P.W. Atkins, Physical Chemistry, Oxford University Press, Oxford, 1982.
[82] S.-H. Song, B. Dick, A. Penzkofer, R. Pokorny, A. Batschauer, L.-O. Essen, J. Photochem. Photobiol. B: Biol. 85 (2006) 1.
[83] G.R. Fleming, Chemical Applications of Ultrafast Spectroscopy, Oxford University Press, New York, 1986.
[84] F. Ammer, A. Penzkofer, P. Weidner, Chem. Phys. 192 (1995) 325.
[85] J. Salbeck, M. Schörner, T. Fuhrmann, Thin Solid Films 417 (2002) 20.
[86] R. Philip, W. Holzer, A. Penzkofer, H. Tillmann, H.-H. Hörhold, Synth. Met. 132 (2003) 297.
[87] M.D. McGehee, A.J. Heeger, Adv. Mater. 12 (2000) 1655.
[88] W. Holzer, A. Penzkofer, T. Schmitt, A. Hartmann, C. Bader, H. Tillmann, D. Raabe, R. Stockmann, H.-H. Hörhold, Opt. Quant. Electron. 33 (2001) 121.
[89] G.J. Denton, N. Tessler, M.A. Stevens, R.H. Friend, Adv. Mater. 9 (1997) 547.
[90] W. Holzer, A. Penzkofer, T. Pertsch, N. Danz, A. Bräuer, E.B. Kley, H. Tillmann, C. Bader, H.-H. Hörhold, Appl. Phys. B 74 (2002) 333.
[91] U. Lemmer, A. Haugeneder, C. Kallinger, J. Feldmann, in: G. Hadziioannou, P. van Hutten (Eds.), Semiconducting Polymers: Chemistry, Physics and Engineering, Wiley–VCH, Weinheim, 1999, p. 309.
[92] S.V. Frolov, M. Shkunov, A. Fujii, K. Yosino, Z.V. Vardeny, IEEE J. Quantum Electron. 36 (2000) 2.
[93] G. Kranzelbinder, G. Leising, Rep. Prog. Phys. 63 (2000) 729.
[94] U. Scherf, S. Riechel, U. Lemmer, R.F. Mahrt, Curr. Opin. Solid State Mater. Sci. 5 (2001) 143.